Energy Transfer Induced by Carbon Quantum Dots in Porous Zinc Oxide Nanocomposite Films

ARTICLE *in* THE JOURNAL OF PHYSICAL CHEMISTRY C · JANUARY 2015

Impact Factor: 4.77 · DOI: 10.1021/jp510661d

9 AUTHORS, INCLUDING:

Luca Malfatti
Università degli Studi di Sassari
107 PUBLICATIONS **1,370** CITATIONS
SEE PROFILE

Alessandro Moretto
University of Padova
90 PUBLICATIONS **1,280** CITATIONS
SEE PROFILE

Masahide Takahashi
Osaka Prefecture University
250 PUBLICATIONS **3,255** CITATIONS
SEE PROFILE

Plinio Innocenzi
Università degli Studi di Sassari
211 PUBLICATIONS **4,833** CITATIONS
SEE PROFILE

THE JOURNAL OF PHYSICAL CHEMISTRY C

Article

pubs.acs.org/JPCC

Energy Transfer Induced by Carbon Quantum Dots in Porous Zinc Oxide Nanocomposite Films

Kazumasa Suzuki,[†,‡,§] Luca Malfatti,[†,§] Davide Carboni,[†] Danilo Loche,[∥] Maria Casula,[∥] Alessandro Moretto,[⊥] Michele Maggini,[⊥] Masahide Takahashi,[‡,§] and Plinio Innocenzi*[,†,§]

[†]Laboratorio di Scienza dei Materiali e Nanotecnologie, D.A.D.U., Università di Sassari, CR-INSTM, Palazzo Pou Salit, Piazza Duomo 6, 07041 Alghero (Sassari), Italy

[‡]Department of Materials Science, Graduate School of Engineering, and [§]International Laboratory of Materials Science and Nanotechnology (iLMNT), Osaka Prefecture University, Sakai, Osaka 599-8531, Japan

[∥]Dipartimento di Scienze Chimiche e Geologiche and INSTM, Università di Cagliari, S.P. Monserrato-Sestu, km 0.700, Monserrato, 09042 Cagliari, Italy

[⊥]Dipartimento di Scienze Chimiche, Università di Padova, Via Marzolo, 1, 35131 Padova, Italy

Supporting Information

ABSTRACT: A one-pot approach making use of a zinc oxide sol precursor and carbon quantum dots, together with a partially fluorinated block copolymer as templating agent, has been used to synthesize a porous matrix characterized by interesting energy transfer properties. The choice of the fluorinated surfactant for inducing the porosity into the inorganic matrix has allowed an easy removal of the templating agent at low temperature, preserving at the same time the functional properties of the carbon quantum dots. The resulting nanocomposite films have been characterized by steady-state 3D mapping that has evidenced a complex behavior as a function of the carbon quantum dots concentration. In particular, the luminescence bands of the zinc oxide matrix appear to be modulated by the broad emission of the carbon quantum dots, which depends on their aggregation state. These results can be thus considered as a step further toward the fine-tuning of the luminescence properties provided by zinc oxide-based nanocomposites as a result of a doping effect due to the presence of carbon quantum dots.

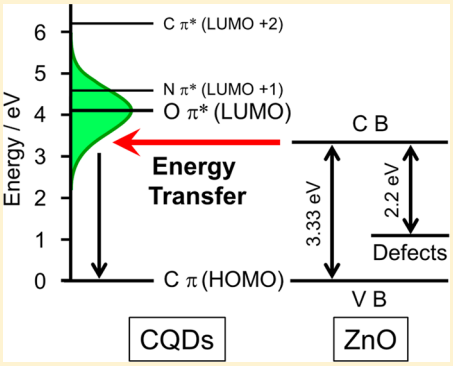

1. INTRODUCTION

Carbon and graphene quantum dots (CQDs and GQDs) have ignited a tremendous research interest as innovative and eco-friendly class of 0D nanomaterials with applications in photonics and optoelectronics.[1] CQDs, in fact, can be regarded as nanometric-sized fragments of graphene, bearing quantum properties similar to semiconductor quantum dots; the combination of pronounced quantum confinement and edge effects, in particular, is responsible for high luminescence. Very recently an increasing number of papers have reported on the use of CQDs for medical imaging as well as for electronic, electrochemical, and photoluminescent sensing.[2] The latter application, in particular, requires a technological improvement in the use of CQDs, that is, the incorporation into matrixes that maximize the interaction of these functional nanostructures with the environment. Sol−gel chemistry in combination with a templating approach based on self-assembly offers a powerful tool for the incorporation of CQDs into thin porous films made by organic−inorganic hybrid or functional oxides. In a previous work, we have successfully embedded physically exfoliated graphene in different systems such as dense silica,[3] mesoporous nanocomposite silica,[4] and mesoporous titania.[5] Noticeably, the material synthesis has shown such flexibility that it has allowed its integration with top-down processes and the fabrication of complex nanocomposites in a single step, for the case of mesoporous silica films with gold nanoparticles for Graphene Surface Enhanced Raman Scattering. In this case, a remarkable increase of the functional properties due to the design of the material at the nanoscale has been observed. The same chemical route should, in principle, allow fabricating new porous nanocomposites containing carbon quantum dots. In particular, the CQDs fluorescence in combination with a proper matrix is expected to enable the development of photo-luminescent materials with new properties. We have therefore prepared nanocrystalline ZnO porous thin films containing CQDs to expand the potential of this synthetic approach.

Nanosized crystalline ZnO structures, in fact, show an exciton emission band in the UV region and a defect-related visible emission in the blue to green region.[6−9] On the other hand, CQDs have a wide emission in the visible range that depends on the presence of defects and/or specific functional groups at the edges.[10] The overlapping of the ZnO and CQDs

Received: October 23, 2014
Revised: January 7, 2015

DOI: 10.1021/jp510661d
J. Phys. Chem. C XXXX, XXX, XXX−XXX

photoluminescence should therefore enable energy and/or charge transfer between the two materials; ZnO/CQDs nanocomposites, for instance, exhibit enhanced photocatalytic activity, allowing for photoinduced charge transfer transitions under visible or UV light irradiation. This phenomenon has been already observed both in bulk materials and in multilayered systems formed by a dense ZnO film covered with a thin layer of CQDs.[11,12] To the best of our knowledge, however, there are no studies regarding the charge transfer between ZnO and CQDs in nanocomposite porous films with the carbon nanostructures finely embedded into the porous matrix.

The optimization of the nanocomposite ZnO-CQDs system is expected to enable the tuning of the photoluminescence properties of ZnO by doping them with cheap and easy-to-prepare fluorophores obtained from an abundant raw material such as carbon.

2. EXPERIMENTAL SECTION

2.1. Chemicals. Zinc acetate dihydrate (Sigma-Aldrich, >99.5%), ethanol (Sigma-Aldrich, >99.8%), water (milli-Q), fluorosurfactant Zonyl FS300 ($RfCH_2CH_2O(CH_2CH_2O)_xH$; $Rf = F(CF_2CF_2)_y$, where $x = 14$ and $y = 3$, ∼40% weight in water, Sigma-Aldrich) were used for preparing porous ZnO film. All reagents were analytical grade and used as received without further purification. Silicon wafers (Si-Mat; 100) cut, p-type boron doped, 350 μm thick, and silica glasses (Heraeus), SUPRASIL 2 grade B, 1 mm thick, were used as substrates for film deposition.

2.2. Synthesis of Carbon Quantum Dots (CQDs). CQDs have been synthesized following an already established method.[13] Arginine·HCl (5.6 g, 26.6 mmol) and 1,2-ethylendiamine (1.78 mL, 26.6 mmol) were dissolved in 13.3 mL of ultrapure water. The solution was placed in a domestic microwave oven and heated at 700 W for 180 s. The brown-burned resulting solid was suspended in 50 mL of ultrapure water and centrifuged several times. The aqueous solution was placed in a dialysis sack (1 KD cutoff) and dialyzed against ultrapure water for 24 h. Finally, the aqueous solution was lyophilized, giving 1.2 g of solid CQDs.

2.3. Synthesis of Mesoporous Zinc Oxide Films with CQDs. Zinc acetate dihydrate (2.2 g, 0.01 mol) and Zonyl FS300 (1.32 g of Zonyl, 1.35 mmol) were mixed in ethanol (12 mL, 0.26 mol) under stirring, and then water (10 mL, 0.56 mol) was finally added. The molar ratios of the final precursor solution of ZnO sol were $Zn(CH_3COO)_2·2H_2O/EtOH/H_2O/Zonyl = 1:26:65:0.135$. The same protocol was followed for the preparation of ZnO-CQD sol; as a final step for the ZnO-CQD sol, increasing amounts of CQD powder (2.5, 5, 10 mg) were added into the precursor sol (10 mL), and ultrasonication was then conducted for 10 min. The sols were left under stirring in a closed vial for 30 min at room temperature before deposition. Films were deposited by spin-coating on silicon wafers and silica glasses in air at the rate of 800 rpm for 20 s. After deposition, the samples were annealed in an oven at 200 °C for 3 h in air.

2.4. Characterization Methods and Instrumentation. *TEM.* Bright field images were obtained by a transmission electron microscope (TEM) JEM-2000FX operating at 200 kV. The samples for analysis were obtained by scratching the films and dispersing them in ethanol. Copper grids were dipped into the sample solution and dried before TEM analysis.

XRD. X-ray diffraction (XRD) patterns were recorded using a Bruker diffractometer D8 Discover working in grazing incidence geometry with a Cu Kα line (λ = 1.54056 Å); the X-ray generator was set at 40 kV and 40 mA. Diffraction patterns were recorded in 2θ ranging from 20 to 80° with a step size of 0.05° and scan speed of 0.5 s/step; the measurements were repeated until a good signal-to-noise ratio was achieved.

Porosimetry. Absorption and desorption isotherms were recorded by using a Quantachrome iQ porosimeter using nitrogen as a probe gas at 77 K. The analyses were performed on mesoporous zinc oxide powders both with CQDs and without CQDs. The powders were obtained by casting the precursor solutions on Petri dishes to obtain thick films that were treated 12 h at 200 °C in an oven in air and then outgassed for 2 h at 100 °C before performing the analysis. The pore size distribution has been calculated using a DFT model applied to the isotherm curves.

FTIR. Fourier-transform infrared (FTIR) analysis was performed with an interferometer Bruker infrared Vertex 70v. The spectra were recorded in transmission mode between 4000 and 400 cm^{-1} by averaging 256 scans with 4 cm^{-1} of resolution. The background was evaluated by measuring the signal of a clean silicon wafer substrate; the baseline was fitted by a concave rubber band correction with OPUS 7.0 software.

UV−Vis. Transmission spectra of the zinc oxide film with 10 mg CQDs and the bare zinc oxide film were measured in the range of 200−700 nm with a bandwidth of 1.5 nm using UV−Vis Nicolet Evolution 300 spectrophotometer.

Fluorescence. Fluorescence spectra were recorded with a "NanoLog" Horiba Jobin Yvon spectrofluorometers: 3D and 2D mapping were recorded with a 450 W xenon lamp as the excitation source. 3D maps were collected with an excitation range of 250−600 nm and an emission range of 300−800 nm. 2D maps were collected exciting at 325 nm and acquiring the emission in the range of 340−700 nm.

Spectroscopic Ellipsometry. A Woollam-α spectroscopic ellipsometer with fixed angle geometry was used for thickness measurements of films deposited on silicon wafers. The thickness was estimated by fitting the experimental data with a Cauchy model for transparent films on Si substrate.

3. RESULTS AND DISCUSSION

The sol−gel synthesis of the ZnO-CQD films has been carefully designed to provide high photoluminescence properties of the nanocomposite material. The choice of the solvent to be employed in the synthesis has been a crucial step; after several attempts, ethanol has been chosen for the precursor solution because, with respect to other organic solvents, it allows dispersing the highest amount of CQDs in the sol. In addition, a nonionic fluorosurfactant (Zonyl FS300) has been selected as a porogen template of the inorganic matrix instead of the most common Pluronic-like block copolymers.[14] Zonyl FS300, in fact, can be easily removed from the films in mild conditions after a thermal treatment at low temperature preserving the luminescence of the CQDs.[15] The recipe for the preparation of CQDs allows obtaining Nitrogen-doped carbon dots of 1−2 nm in diameter through microwave-assisted transformation of arginine in the presence of ethylenediamine. This procedure has been chosen because it allows producing highly fluorescent CQDs. The photophysical properties of CQDs, obtained by this recipe, have been studied in solution in previous papers.[16] It has been observed, in particular, that the

DOI: 10.1021/jp510661d
J. Phys. Chem. C XXXX, XXX, XXX−XXX

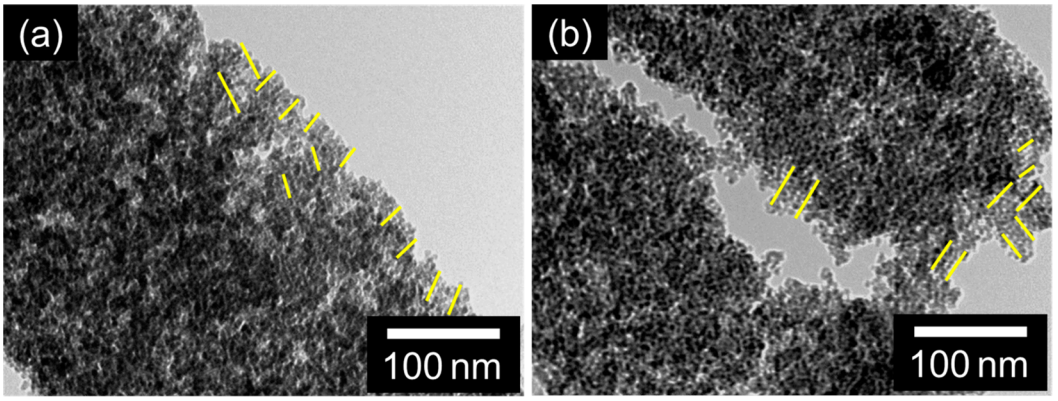

Figure 1. Bright field TEM pictures of ZnO-CQD (10 mg) and ZnO films treated at 200 °C (a, b). Partially oriented porous domains have been highlighted by yellow lines.

quantum yield and lifetime of the photoluminescence increases with increasing nitrogen content.

Figure 1 shows the TEM images of a representative ZnO-CQD films (Figure 1a) in comparison with a bare porous ZnO (Figure 1b) after treatment at 200 °C in air. The sol used for the deposition of the two films is identical, except for the addition of CQDs in a concentration of 10 mg in 10 mL of solution. The pore walls are interconnected nanocrystalline ZnO particles with a size ranging from 5 to 8 nm, as measured by line plot profile on bright field pictures (Supporting Information, Figure S1). The addition of CQDs does not affect the final morphology of the material. However, in both cases no long-range organization of the pores has been observed and only limited domains of the inorganic matrix have a porosity with local order. CQDs are barely visible in the inorganic matrix because of their low electron contrast.

The crystalline structure of the films after treatment at 200 °C has been further confirmed by X-ray diffraction (Figure 2); a

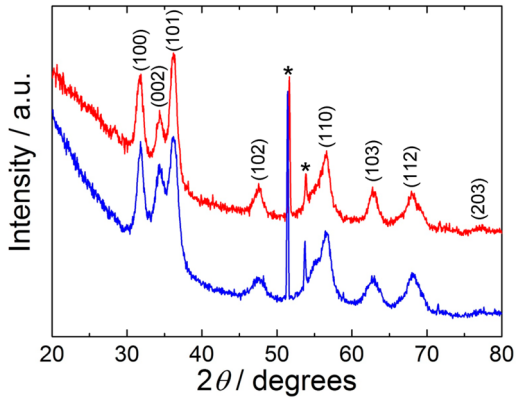

Figure 2. XRD patterns of the ZnO-CQD (10 mg) and ZnO (red and blue line) films. The asterisks refer to the monocrystalline Si wafer used as the substrate.

comparison between the sample containing CQDs (10 mg) with that one made of pure ZnO clearly shows that the addition of the carbon-based nanostructures does not affect the crystallization kinetic of the films. In fact, the characteristic diffraction peaks of the Wurtzite-like phase[17] are present in both diffraction patterns with comparable relative intensities. Scherrer's equation has been applied to the patterns to estimate the crystal size; values of 8.2 and 6.0 nm for the CQDs-functionalized and the bare ZnO film, respectively, have been obtained. The result is in agreement with TEM measurements. Similar results have been also obtained with nanocomposite samples with intermediate CQD concentrations (not shown in figures).

N_2 adsorption/desorption isotherms have been used to measure the surface area, pore size and volume on pure ZnO and CQD-doped ZnO nanocomposites. Figure 3a and b show the results for ZnO-CQD (10 mg) and ZnO after treatment at 200 °C, respectively. Following the IUPAC classification, both samples show a type-IV isotherm with a type H4 hysteresis loop typical of the physisorption in a mesoporous matrix.[18] This trend is typical of organic−inorganic nanocomposites when the size of the pores is close to the micropore range.[19] Both samples, in fact, have a polydispersed pore size distribution with micropores of about 1.8−1.9 nm dimension and mesopores of about 3.6−3.8 nm. The dimension of mesopores is similar to that one previously obtained in Zonyl-templated porous materials,[15] while the micropores are likely due to a collapse of the mesoporous structure as a consequence of the ZnO crystallization at low temperature. BET analysis allows estimating the surface area of the samples as 29 m^2 g^{-1} for the ZnO and 7 m^2 g^{-1} for the ZnO-CQD. Despite the similar dimension of crystal, the surface area of ZnO-CQD is smaller than that of ZnO; the addition of CQDs, in fact, could have contributed to the mesopore collapse by affecting the mechanical stability of the inorganic matrix.

Spectroscopic ellipsometry has been used to measure the nanocomposite film thickness with respect to the bare ZnO samples as a function of the temperature (see Supporting Information, Table S1). The addition of the CQDs to the sol for the film deposition is responsible for an increase of the final thickness of the coating which is attributed to a different viscosity in the sol due to the CQDs addition. After treatment at 200 °C, in particular, the ZnO sample shows a thickness of ≈124 nm, while the CQDs addition in the sol causes an increase in the thickness of the ZnO-CQD film (10 mg) up to ≈157 nm.

FTIR spectroscopy has been used to monitor the chemical changes in the nanocomposite matrix as a function of the processing temperature. Figure 4 shows the FTIR spectra of a ZnO-CQD film, prepared with 10 mg of carbon quantum dots, as a function of the thermal treatment. Within the 1500−1000 cm^{-1} (Figure 4a), four characteristic bands of the Zonyl fluorosurfactant can be identified in the spectrum of the film; 1240 and 1210 cm^{-1}, attributed to antisymmetric and symmetric stretching of the $-CF_2-$ group,[20] and 1146 and

DOI: 10.1021/jp510661d
J. Phys. Chem. C XXXX, XXX, XXX−XXX

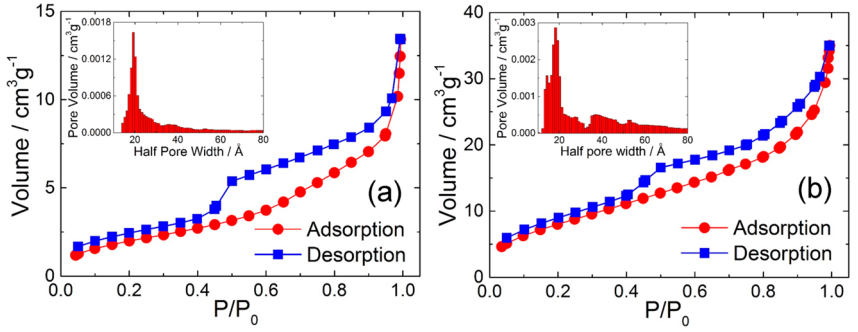

Figure 3. N_2 adsorption/desorption isotherms for ZnO-CQD (10 mg) and pure ZnO samples (a, b). The insets show the pore radius distribution using DFT model.

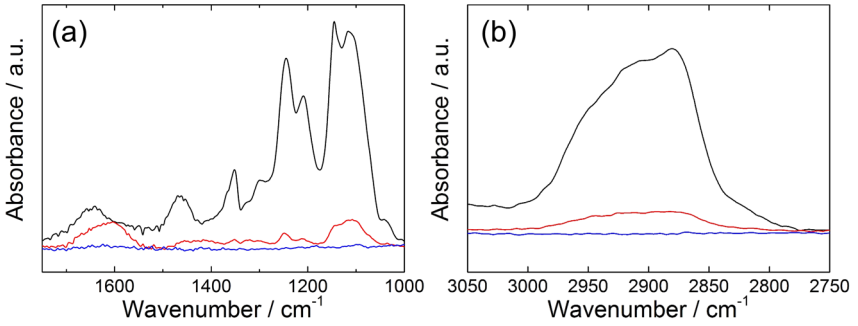

Figure 4. FTIR spectra as a function of the annealing temperature of ZnO-CQD films (10 mg): 100 °C (black line), 200 °C (red line), and 300 °C (blue line).

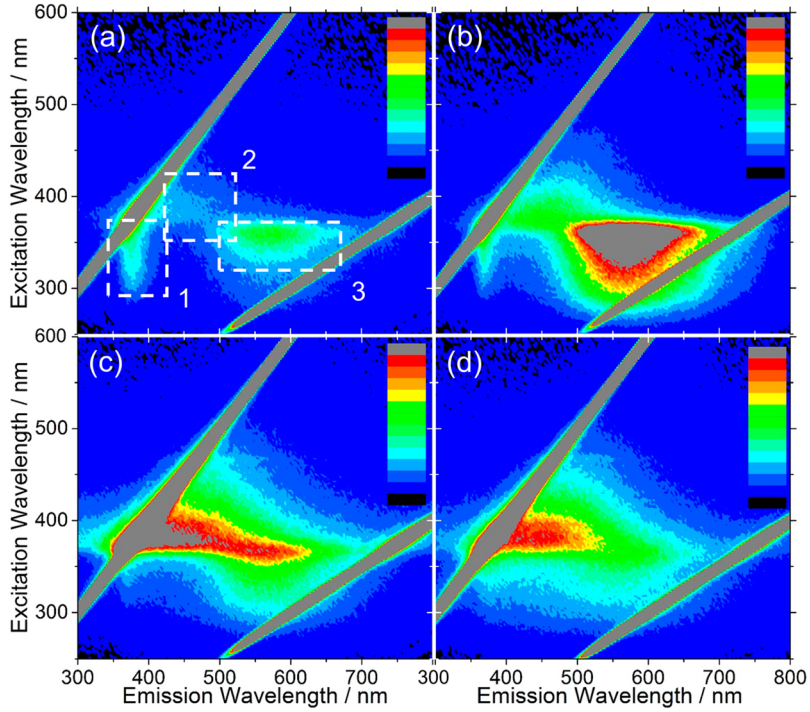

Figure 5. 3D excitation−emission−intensity maps of ZnO nanocomposite films treated at 200 °C as a function of CQD concentration in the sol: (a) pure ZnO, (b) 2.5 mg, (c) 5 mg, (d) and 10 mg CQDs. The photoluminescence intensity is reported in false color scale.

1117 cm^{-1} due to C−C and C−O−C stretching of the ethylene chain.[21] These bands are clearly visible in the spectrum of the sample treated at 100 °C; however, the use of nonionic and fluorinated block copolymer allows for an easy removal of the surfactant at temperatures lower than 300 °C. In fact, after treating the sample in an oven at 200 °C for 3 h, the three bands almost disappear (1240, 1210, and 1145 cm^{-1}), while a weak absorption band, peaked around 1110 cm^{-1}, is still visible in the spectrum. The broad bands relative to CH_2 and CH_3 stretching and peaked at around 2890 cm^{-1} strongly decrease after treatment at 200 °C, indicating an almost complete removal of the organic surfactant (Figure 4b).

DOI: 10.1021/jp510661d
J. Phys. Chem. C XXXX, XXX, XXX−XXX

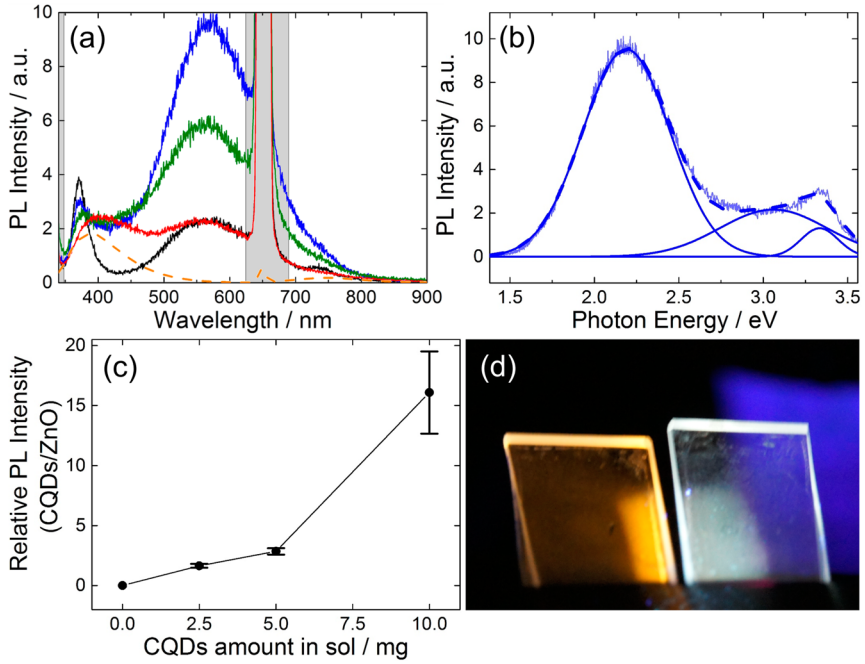

Figure 6. (a) Photoluminescence spectra of the ZnO-CQD films as a function of CQD concentrations (excitation wavelength = 325 nm): bare ZnO (black line), ZnO-CQD 2.5 mg (blue line), ZnO-CQD 5 mg (green line), and ZnO-CQD 10 mg (red line). The CQDs photoluminescence in water is also reported as a reference (dotted orange line). The ranges of the scattering incident light and its second harmonics (<348 nm and 625−690 nm) are shown as gray shadows. (b) A typical result of deconvolution of the PL spectra of ZnO-CQD 2.5 mg (excitation wavelength = 325 nm). (c) Relative PL intensity of CQDs to ZnO as a function of CQD concentrations. (d) A photo image of 2.5 mg (left) and 5 mg (right) of CQD-doped ZnO films under 376 nm light illumination.

The N-doped CQDs we have used for the synthesis, show specific infrared bands that are due to the presence of an amino group in the carbon dots structure. The signal related to the surface amino group of CQDs, N−H bending (1625 cm^{-1}) and stretching (3318 cm^{-1}) modes, and C−N stretching of the amide group (1406 cm^{-1}) have been detected by the ATR infrared spectrum of the CQDs (Figure S2c). The presence of the CQDs in ZnO films after treatment at 200 °C, therefore, has been confirmed by checking the presence of the band peaked around 1600 cm^{-1}, assigned to the N−H bending mode (Figure 4a). The infrared spectra of the sample on the 4000−400 cm^{-1} range and the spectra of Zonyl FS300 and CQDs are reported as Supporting Information (Figure S2a−c).

By comparison, the UV−vis transmission spectrum of the nanocomposite ZnO-CQD film (10 mg CQDs in 10 mL of sol) treated at 200 °C is similar to that of pure ZnO film (Figure S3), and we observe that the change of transmission caused by the highest addition of CQDs (10 mg) is less than 1% at the wavelength range of ZnO PL and the two spectra appear similar. This has been attributed to the broad absorption due to the carbon nanoparticles, which does not show defined peaks (inset of Figure S3).[22,23]

The 3D spectra, illustrating excitation−emission−intensity of the ZnO-CQD films as a function of increasing carbon dots concentration, reveal a complex interplay between the inorganic matrix and the guest nanoparticles (Figure 5). In the 3D plots, in fact, three specific areas can be identified: The first one (area 1; 290−375 nm range in excitation, 350−425 nm range in emission) is attributed to the exciton band of ZnO. The peak in this region is clearly detected in the bare ZnO (Figure 5a) and decreases linearly in relative intensity with the increase of the CQD concentration. The second area (area 2; 350−425 nm range in excitation, 425−525 nm range in emission) is instead assigned to a characteristic emission of the carbon quantum dots. The luminescence in this region follows a complex trend; it is barely detectable in the ZnO film and increases in relative intensity with the increased amount of CQDs up to 5 mg (Figure 5b,c); beyond this concentration value, the relative intensity decreases. The origin of luminescence in the visible range, that is the third region (area 3; 320−375 nm range in excitation, 500−670 nm range in emission), is due to defects on the surface or in the crystal structure of zinc oxide crystallites.[24] The luminescence of this area can be detected in the bare ZnO film and increases in relative intensity after the addition of 2.5 mg of CQDs. A further increase of the dots concentration (5 mg) causes a quenching of the relative intensity, foreseeing a trend that is further confirmed at higher concentrations (10 mg).

The trend of the luminescence in area 1 likely involves concurrent processes, including dipole−dipole interactions (Förster resonance energy transfer, FRET) and reabsorption between ZnO and CQDs, which are simultaneously contributing to the change of PL of the nanocomposite films. To highlight the effect of the energy transfer mechanism, we have plotted the emission spectra, obtained by exciting at 325 nm, as a function of the CQD concentration (Figure 6a). The emission of CQDs in water peaked at 392 nm is also shown as a dotted orange line for comparison.

To get more detailed information about the effect of CQDs addition in the nanocomposite films, a deconvolution analysis have been performed on the PL spectra using Gaussian curves and a typical result of deconvolution is shown in Figure 6b (deconvolution of all the PL spectra as a function of the CQD concentrations are shown in Figure S4). By fitting the PL spectrum of bare ZnO with two Gaussian curves (Figure S4a), we have obtained the peak positions of the bands attributed to

DOI: 10.1021/jp510661d
J. Phys. Chem. C XXXX, XXX, XXX−XXX

exciton and defects, 3.33 and 2.2 eV, corresponding to 372 and 564 nm, respectively. The peak position of the exciton band has been kept as a fixed parameter for comparison of PL spectra related to the samples with increasing amounts of CQDs (Figure S4b–d), while the band peak attributed to defects in the ZnO matrix has been set as free parameter for the iterative fitting processes. The peak position of the band related to CQDs (3.06 eV = 405 nm) have been determined from the deconvolution of the PL spectrum of the sample containing the highest amount of CQDs (10 mg, Figure S4d) with three Gaussian curves. This wavelength value (405 nm) is longer than 392 nm, which is the peak position of the CQDs in water. The CQDs environment affects the photoluminescence properties of the CQDs; therefore, it is reasonable to have this energy shift in the oxide matrix, and a similar shift has been already reported for CQDs embedded in silica matrix.[25]

Figure 6c shows intensity ratio of PLs at 3.06 (CQDs) to 3.33 eV (ZnO) are plotted as a function of CQD concentration. The CQDs/ZnO PL ratio increases nonlinearly with CQDs incorporation. For example, the relative PL ratio increases four times passing from the sample prepared with 5 mg up to samples prepared with 10 mg of CQDs. This nonlinear correlation may indicate that the specific interaction between ZnO and CQDs, such as excitation energy transfer through dipole interactions, has been established. By comparing the band gap of ZnO with respect to HOMO–LUMO gap of CQDs, an energy transfer through dipole resonance mechanisms from ZnO conduction band (CB) to O π^* of CQDs could be expected. The process resumed in the schematic is shown in Figure 7.[26]

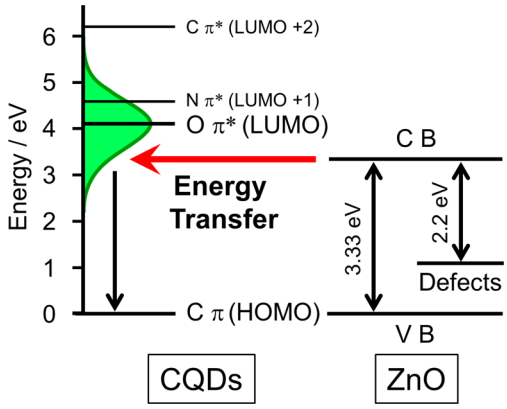

Figure 7. Schematic of the energy transfer mechanism between ZnO and CQDs. The energy level of CQDs are reproduced from ref 26.

Reabsorption of ZnO PL by CQDs may also take place, leading to a decrease of ZnO PL in area 1; however, this interaction cannot be considered as a dominant pathway for the energy transfer, because the addition of the highest amount of CQDs in the ZnO matrix resulted in a <1% decrease of the film transmission at the wavelength range of ZnO PL (Figure S3).

The luminescence intensity in area 2 is typical of CQDs and, up to 5 mg of concentration in the sol, shows an almost linear increase. Beyond this threshold the concentration is quenched likely because of the formation of aggregates in the films. A similar quenching effect has been also observed in liquid phase, by measuring the luminescence properties of the sol as a function of the CQDs concentration (see Supporting Information, Figure S5).

Despite the previous cases, the trend of the luminescence attributed to ZnO defects (area 3) appears of particular complexity and further experiments are ongoing to gain a deeper insight into the system. However, a tentative explanation of the phenomenon can be given by supposing that the interface between ZnO and CQDs could play a role in the formation of the surface defects accountable for the luminescence. At lower concentration, the CQDs are finely dispersed in the inorganic matrix, maximizing the carbon-inorganic interface. As soon as the concentration rises in the sol, the carbon dots starts aggregating, as confirmed by the quenching of characteristic luminescence. The formation of aggregates decreases the active interface between carbon and zinc oxide crystals, thus reducing the enhancement of photoluminescence.

A photo image of CQD-doped ZnO films (2.5 and 5 mg CQDs added) under 376 nm light illumination is shown in Figure 6d. Both films showed apparent fluorescence, but the colors are clearly different. The film doped with 2.5 mg of CQDs shows orange color, but that with 5 mg emits white light PL. Highly doped composites show white light PL because the wide bandwidth exceeds over several hundred nanometer. The CQDs doping into ZnO matrix enables us to achieve the wavelength tuning of the PL in wide visible wavelength range. Considering the UV tunable downconverting property and broad nature of PL band, implementation of this materials into functional devices can be foreseen; in particular application in solar cell systems for harvesting UV components of the sun light, UV shielding windows and phosphors for lighting application.

4. CONCLUSIONS

Zinc oxide porous films containing carbon quantum dots have been successfully prepared through a one-pot method based on sol–gel chemistry. The fluorosurfactant used as a templating agent can be easily removed after treatment at 200 °C leaving an accessible porosity. The thermal treatment, at the same time, allows preserving the photoluminescence properties of the carbon quantum dots, enabling multiple effects due to interplay between the semiconductor matrix and the luminescent nanoparticles. The complex trend shown by 3D photoluminescence measurements has been attributed to energy transfer involving dipole interactions and reabsorption between ZnO and CQDs, and formation of surface defects in the inorganic oxide structure. The present work can be regarded as the first step toward the engineering at the nanoscale of complex composite systems based on the synergy between functional oxides and carbon quantum dots. The optimization of the nanocomposite ZnO-CQD system is expected to enable the tuning of the photoluminescence properties of ZnO by doping them with cheap and easy-to-prepare fluorophores obtained from an abundant raw material such as carbon.

■ ASSOCIATED CONTENT

Supporting Information

Line plot profile of the ZnO nanocrystals on TEM image (Figure S1); FTIR spectra of ZnO-CQD films in the 4000–400 cm^{-1} range as a function of the thermal treatment (Figure S2a); FTIR spectrum of Zonyl fluorosurfactant casted on Si substrate (Figure S2b); ATR infrared spectrum of CQDs in powder (Figure S2c); UV–Vis spectra of ZnO-CQD and ZnO films treated at 200 °C and CQDs in water (Figure S3); Deconvolution analysis for the photoluminescence spectra of

DOI: 10.1021/jp510661d
J. Phys. Chem. C XXXX, XXX, XXX–XXX

ZnO-CQD films prepared at increasing CQDs concentration (Figure S4); 3D excitation−emission−intensity maps of ZnO sols as a function of CQDs concentration (Figure S5); Table of the ZnO-CQD and ZnO film thickness as a function of the thermal treatment (Table S1). This material is available free of charge via the Internet at http://pubs.acs.org.

AUTHOR INFORMATION

Corresponding Author

*E-mail: plinio@uniss.it.

Notes

The authors declare no competing financial interest.

ACKNOWLEDGMENTS

D.C. acknowledges the financial support by the Sardinian Regional Government (P.O.R. SARDEGNA F.S.E. 2007-2013 - Obiettivo competitività regionale e occupazione, Asse IV Capitale umano, Linea di Attività l.3.1.). M.M. acknowledges the financial support by MIUR (FIRB *Nanosolar*, RBAP11C58Y_004). M.T. acknowledges the financial support by JSPS "Brain Circulation" Project (R2507) and University of Sassari "visiting scientist program"

REFERENCES

(1) Li, L.; Wu, G.; Yang, G.; Peng, J.; Zhao, J.; Zhu, J.-J. Focusing on Luminescent Graphene Quantum Dots: Current Status and Future Perspectives. *Nanoscale* **2013**, *5*, 4015−4039.

(2) Sun, H.; Wu, L.; Wei, W.; Qu, X. Recent Advances in Graphene Quantum Dots for Sensing. *Mater. Today* **2013**, *16*, 433−442.

(3) Innocenzi, P.; Malfatti, L.; Lasio, B.; Pinna, A.; Loche, D.; Casula, M. F.; Alzari, V.; Mariani, A. Sol-Gel Chemistry for Graphene−Silica Nanocomposite Films. *New J. Chem.* **2014**, *38*, 3777−3782.

(4) Carboni, D.; Lasio, B.; Alzari, V.; Mariani, A.; Loche, D.; Casula, M.; Malfatti, L.; Innocenzi, P. Graphene-Mediated Surface Enhanced Raman Scattering in Silica Mesoporous Nanocomposite Films. *Phys. Chem. Chem. Phys.* **2014**, *16*, 25809−25818.

(5) Malfatti, L.; Falcaro, P.; Pinna, A.; Lasio, B.; Casula, M. F.; Loche, D.; Falqui, A.; Marmiroli, B.; Amenitsch, H.; Sanna, R.; et al. Exfoliated Graphene into Highly Ordered Mesoporous Titania Films: Highly Performing Nanocomposites from Integrated Processing. *ACS Appl. Mater. Interfaces* **2014**, *6*, 795−802.

(6) Vanheusden, K.; Warren, W. L.; Seager, C. H.; Tallant, D. R.; Voigt, J. A.; B.E. Gnade, B. E. Mechanisms behind Green Photoluminescence in ZnO Phosphor Powders. *J. Appl. Phys.* **1996**, *79*, 7983−7990.

(7) Sakohara, S.; Ishida, M.; Anderson, M. A. Visible Luminescence and Surface Properties of Nanosized ZnO Colloids Prepared by Hydrolyzing Zinc Acetate. *J. Phys. Chem. B* **1998**, *102*, 10169−10175.

(8) Leiter, F. H.; Alves, H. R.; Hofstaetter, A.; Hofmann, D. H.; Meyer, B. K. The Oxygen Vacancy as the Origin of a Green Emission in Undoped ZnO. *Phys. Stat. Sol. B* **2001**, *226*, R4−R5.

(9) Norberg, N. S.; Gamelin, D. R. Influence of Surface Modification on the Luminescence of Colloidal ZnO Nanocrystals. *J. Phys. Chem. B* **2005**, *109*, 20810−20816.

(10) Bourlinos, A. B.; Stassinopoulos, A.; Anglos, D.; Zboril, R.; Karakassides, M.; Giannelis, E. P. Surface Functionalized Carbogenic Quantum Dots. *Small* **2008**, *4*, 455−458.

(11) Yu, H.; Zhang, H.; Huang, H.; Liu, Y.; Li, H.; Ming, H.; Kang, Z. ZnO/Carbon Quantum Dots Nanocomposites: One-Step Fabrication and Superior Photocatalytic Ability for Toxic Gas Degradation under Visible Light at Room Temperature. *New J. Chem.* **2012**, *36*, 1031−1035.

(12) Li, Y.; Zhang, B.-P.; Zhao, J.-X.; Ge, Z.-H.; Zhao, X.-K.; Zou, L. ZnO/Carbon Quantum Dots Heterostructure with Enhanced Photocatalytic Properties. *Appl. Surf. Sci.* **2013**, *279*, 367−373.

(13) Mazzier, D.; Favaro, M.; Agnoli, S.; Silvestrini, S.; Granozzi, G.; Maggini, M.; Moretto, A. Synthesis of Luminescent 3D Microstructures Formed by Carbon Quantum Dots and Their Self-Assembly Properties. *Chem. Commun.* **2014**, *50*, 6592−6595.

(14) Innocenzi, P.; Malfatti, L.; Piccinini, M.; Marcelli, C. Evaporation-Induced Crystallization of Pluronic F127 Studied in Situ by Time-Resolved Infrared Spectroscopy. *J. Phys. Chem. A* **2010**, *114*, 304−308.

(15) Carboni, D.; Marongiu, D.; Rassu, P.; Pinna, A.; Amenitsch, H.; Casula, M.; Marcelli, A.; Cibin, G.; Falcaro, P.; Malfatti, L.; et al. Enhanced Photocatalytic Activity in Low-Temperature Processed Titania Mesoporous Films. *J. Phys. Chem. C* **2014**, *118*, 12000−12009.

(16) Zhai, X.; Zhang, P.; Liu, C.; Bai, T.; Li, W.; Dai, L.; Liu, W. Highly Luminescent Carbon Nanodots by Microwave-Assisted Pyrolysis. *Chem. Commun.* **2012**, *48*, 7955−7957.

(17) JCDD, International Centre for Diffraction Data, *PDF Database, Card No. 80−0074.*

(18) Kruk, M.; Jaroniec, M. Gas Adsorption Characterization of Ordered Organic−Inorganic Nanocomposite Materials. *Chem. Mater.* **2001**, *13*, 3169−3183.

(19) Sing, K. S. W.; Everett, D. H.; Haul, R. A. W.; Moscou, L.; Pierotti, R. A.; Rouquerol, J.; Siemieniewska, T. Reporting Physisorption Data for Gas/Solid Systems with Special Reference to the Determination of Surface Area and Porosity. *Pure Appl. Chem.* **1985**, *57*, 603−619.

(20) Lin-Vien, D.; Colthup, N. B.; Fateley, W. G.; Grasselli, J. G. *The Handbook of Infrared and Raman Characteristic Frequencies of Organic Molecules*; Academic Press: San Diego, CA, 1991.

(21) Su, Y.-L.; Wang, J.; Liu, H.-Z. FTIR Spectroscopic Investigation of Effects of Temperature and Concentration on PEO-PPO-PEO Block Copolymer Properties in Aqueous Solutions. *Macromolecules* **2002**, *35*, 6426−6431.

(22) Sun, Y. P.; Zhou, B.; Lin, Y.; Wang, W.; Fernando, K. A. S.; Pathak, P.; Meziani, M. J.; Harruff, B. A.; Wang, X.; Wang, H.; et al. Quantum-Sized Carbon Dots for Bright and Colorful Photoluminescence. *J. Am. Chem. Soc.* **2006**, *128*, 7756−7757.

(23) Zhou, J.; Booker, C.; Li, R.; Zhou, X.; Sham, T.-K.; Sun, X.; Ding, Z. An Electrochemical Avenue to Blue Luminescent Nanocrystals from Multiwalled Carbon Nanotubes (MWCNTs). *J. Am. Chem. Soc.* **2007**, *129*, 744−745.

(24) van Dijken, A.; Meulenkamp, E. A.; Vanmaekelbergh, D.; Meijerink, A. The Luminescence of Nanocrystalline ZnO Particles: The Mechanism of the Ultraviolet and Visible Emission. *J. Lumin.* **2000**, *87−89*, 454−456.

(25) Zong, J.; Zhu, Y.; Yang, X.; Shen, J.; Li, C. Synthesis of Photoluminescent Carbogenic Dots using Mesoporous Silica Spheres as Nanoreactors. *Chem. Commun.* **2011**, *47*, 764−766.

(26) Tang, L.; Ji, R.; Li, X.; Teng, K. S.; Lau, S. P. Energy-Level Structure of Nitrogen-Doped Graphene Quantum Dots. *J. Mater. Chem. C* **2013**, *1*, 4908−4915.

DOI: 10.1021/jp510661d
J. Phys. Chem. C XXXX, XXX, XXX−XXX